35th Annual International Conference of the IEEE EMBS
Osaka, Japan, 3 - 7 July, 2013

Estimation of Aortic Pressure Waveforms from 4D Phase-Contrast MRI

Michael Delles, Fabian Rengier, Yoo-Jin Jeong, Hendrik von Tengg-Kobligk, Sebastian Ley, Hans-Ulrich Kauczor, Rüdiger Dillmann, and Roland Unterhinninghofen

Abstract— **Several approaches for the non-invasive MRI-based measurement of the aortic pressure waveform over the heart cycle have been proposed in the last years. These methods are normally based on time-resolved, two-dimensional phase-contrast sequences with uni-directionally encoded velocities (2D PC-MRI). In contrast, three-dimensional acquisitions with tri-directional velocity encoding (4D PC-MRI) have been shown to be a suitable data source for detailed investigations of blood flow and spatial blood pressure maps. In order to avoid additional MR acquisitions, it would be advantageous if the aortic pressure waveform could also be computed from this particular form of MRI. Therefore, we propose an approach for the computation of the aortic pressure waveform which can be completely performed using 4D PC-MRI. After the application of a segmentation algorithm, the approach automatically computes the aortic pressure waveform without any manual steps. We show that our method agrees well with catheter measurements in an experimental phantom setup and produces physiologically realistic results in three healthy volunteers.**

I. INTRODUCTION

PATIENT-SPECIFIC knowledge of the development of the aortic blood pressure over a heart cycle is of great clinical interest. Methods for non-invasive computation of the aortic pressure waveform (APW) from blood flow measurements by phase-contrast magnetic resonance imaging (PC-MRI) are promising. In these algorithms, the mean pulse wave velocity (PWV) is computed first. Secondly, the APW of a chosen vessel section is calculated. All computations are based on time-resolved values of blood flow Q and area A of several vessel cross-sections. These parameters can be acquired by time-resolved, two-dimensional phase-contrast sequences with uni-directionally encoded velocities (2D PC-MRI) [1]. For example, the PWV can be computed from Q and A using either a wave equation [2] or the observed delay in the pulse arrival times at different locations along the vessel section [1]. Subsequently, the APW can be calculated using the Moens-Korteweg equation [2].

Computing the APW from three-dimensional MRI with tri-directional velocity encoding (4D PC-MRI) would have the advantage that additional detailed investigations of the blood flow and computations of spatial pressure maps [3] can be performed on the same imaging data. On the other hand, 4D PC-MRI typically suffers from a low temporal resolution. Thus, the blood flow Q of multiple, manually-placed analysis planes on vessel cross-sections in the 4D image volume has to be investigated in order to achieve robust results for the PWV [4,5]. To our knowledge, no methods for the computation of the APW based on 4D PC-MRI have been presented yet.

In this article, we present a method for the robust computation of the APW from 4D PC-MRI. The method is based on the same principles as the work of Markl et al. [4] for the computation of the PWV and Urchuk et al. [2], who computed the APW from 2D PC-MRI on vessel cross-sections. All process steps of our method are implemented in our in-house developed software framework [6]. After the application of a segmentation algorithm, the approach automatically computes the APW without any manual steps. This is possible due to the automatic placement of cross-sectional analysis planes in the 4D PC-MR image volumes. We validate our method using MR images of an experimental phantom setup and reference measurements given by catheterization. Additionally, we apply our approach to MRI acquisitions of three healthy volunteers. In all experiments, we assess the impact of different definitions of the pulse arrival time. Finally, we also investigate the relationship between the number of cross-sectional analysis planes and the accuracy of the results of our approach.

II. METHODS

A. MRI and Preprocessing

Initially, the 4D MR image volumes are imported into our in-house developed software framework, in which all further computational steps are carried out. The time-resolved 3D field of flow vectors is corrected for remaining phase-offset errors. Subsequently, the vessel volume and centerline are identified by applying a semi-automated segmentation algorithm [7], which is based on both the morphological information and the tri-directional velocity information of 4D PC-MRI. For an arbitrary position on the centerline, given by a scalar curve parameter d, the software automatically calculates the 6D pose of the corresponding cross-sectional analysis plane. For each cross-sectional analysis plane, the

M. Delles, Y. Jeong, R. Dillmann, R. Unterhinninghofen are with the Institute for Anthropomatics, Karlsruhe Institute of Technology (KIT), Karlsruhe, Germany. (email: delles@kit.edu)

F. Rengier is with the Department of Diagnostic and Interventional Radiology, University Hospital Heidelberg, Heidelberg, Germany and with the Department of Radiology E010, German Cancer Research Center (dkfz), Heidelberg, Germany.

H. von Tengg-Kobligk is with the Department of Diagnostic and Interventional Radiology, University Hospital Heidelberg, Heidelberg, Germany and with the Department of Radiology E010, German Cancer Research Center (dkfz), Heidelberg, Germany and with the HVTK, Department of Diagnostic, Interventional and Pediatric Radiology, Inselspital, Bern, Switzerland.

S. Ley, H.U. Kauczor are with the Department of Diagnostic and Interventional Radiology, University Hospital Heidelberg, Heidelberg, Germany.

Michael Delles was funded by the German Research Foundation within the setting of "DFG Grant UN 306/1-1". Fabian Rengier and Yoo-Jin Jeong received a grant from the German Research Foundation within the "Research training group 1126".

software computes values of the flow Q and area A from the PC-MRI velocity field for each time step t in the heart cycle T. By this means, two-dimensional scalar fields $Q(d,t)$ and $A(d,t)$ $(d \in D, t \in T)$ are calculated for a chosen section D of the vessel centerline without any manual user interaction (see Fig. 1). The resolution in the temporal dimension is linearly interpolated to 5 ms. The resolution Δd in the spatial dimension is specified by the number of analysis planes and can be arbitrarily chosen in our software.

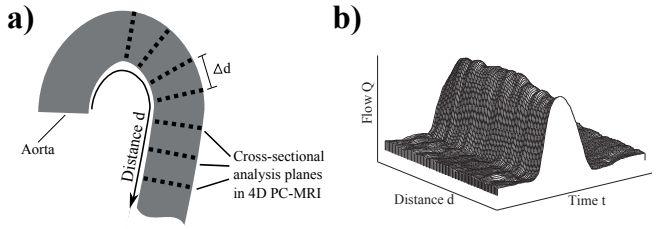

Fig. 1. a) Schematical view of cross-sectional analysis planes in the 4D PC-MRI volume. b) Example for the resulting flow field Q.

B. Computation of the Pulse Wave Velocity

The computation of the mean PWV of the chosen vessel section D is based on the pulse arrival time, which is defined as the time of occurence of a certain feature in the flow $Q(d_i,t)$ of a cross-sectional analysis plane d_i. Commonly, the foot of the systolic upstroke is said to be the most robust flow feature, if wave reflections are possible [8]. The determination of the foot relies on computing a regression line r_i for the systolic upstroke of the flow for a given value d_i. The upstroke regression line r_i is computed from the flow values $Q(d_i,t)$ at all points in time t which fulfill two different criteria. First, only the flow values from the early systole $(t \in [t_p - T/3\,,\, t_p])$ prior to the systolic peak t_p are used. Second, the flow values $Q(d_i,t)$ have to fulfill $Q_\alpha(d_i) \leq Q(d_i,t) \leq Q_\beta(d_i)$ with

$$Q_\alpha(d_i) = Q_{min}(d_i) + \alpha * (Q_{max}(d_i) - Q_{min}(d_i)) \quad (1)$$

$$Q_\beta(d_i) = Q_{min}(d_i) + \beta * (Q_{max}(d_i) - Q_{min}(d_i)) \quad (2)$$

$$Q_{min}(d_i) = \min_{t \in T} Q(d_i,t) \quad (3)$$

$$Q_{max}(d_i) = \max_{t \in T} Q(d_i,t) \quad . \quad (4)$$

The diastolic horizontal line s_i is defined by averaging the flow values $Q(d_i,t)$ at all points in time t where $Q(d_i,t) < Q_\alpha(d_i)$ holds. In all experiments of the presented article, $\alpha = 0.3$ and $\beta = 0.7$ were used. The *Foot* pulse arrival time t_i is defined as the intersection of r_i with the horizontal line s_i of the mean diastolic flow value. For comparison purposes, we also investigated another definition of the pulse arrival time (*Foot'*, $t_{i'}$) , where the regression line r_i is intersected with the zero baseline. The methods for obtaining the two pulse arrival times are illustrated in Fig. 2.

The pulse arrival times t_i or $t_{i'}$ are computed for all analysis planes d_i. From the plot of t_i as a function of d_i,

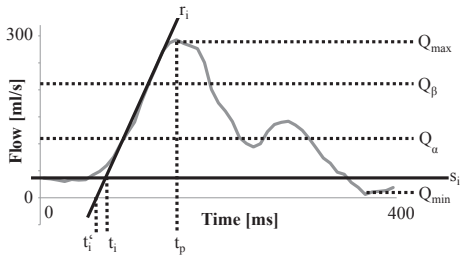

Fig. 2. Computation of the two different pulse arrival times. Only the systolic part of a heart cycle is shown.

the PWV c is defined as the reciprocal value of the slope of a linear fit to the data [4]. By using the pulse arrival times of a large number of analysis planes, the mean PWV c of the vessel section D can be robustly computed despite the low temporal resolution of the 4D flow measurements.

C. Computation of the Aortic Pressure Waveform

Using the same physical background as Urchuk et al. [6], we compute the APW $p_{stat}(d,t)$ of the relative static pressure at each cross-section d. The term "relative" indicates that all approaches are only able to deliver the temporal change in the spatially averaged static blood pressure, while its absolute height remains unknown. Integrating the general expression

$$\frac{\partial p_{stat}(d,t)}{\partial t} = \frac{\partial p_{stat}(d,t)}{\partial A} \cdot \frac{\partial A(d,t)}{\partial t} \quad (5)$$

and using the formula of Moens-Korteweg, (5) can be rewritten as

$$p_{stat}(d,t) = \frac{\rho}{\frac{1}{|T|}\sum_{t \in T} A(d,t)} \cdot c^2 \cdot A(d,t) \quad (6)$$

with the blood density $\rho = 1060 \frac{kg}{m^3}$, the two-dimensional field A of the cross-sectional areas and the previously computed PWV c. The APW $p_{stat}(t)$ of the spatially averaged, relative, static pressure in the vessel section D is computed by averaging the temporal pressure variations $p_{stat}(d,t)$ from (6) at every cross-section $d \in D$.

D. In-Vitro Study: Experimental Phantom Setup

We evaluated our approach using an experimental phantom setup [9,10]. It represents pulsatile blood flow in the human descending aorta. Using a computer-controlled pump and a blood mimicking fluid, realistic aortic flow and pressure conditions are achieved in a straight elastic tube with a diameter of 30 mm. We performed 4D PC-MRI acquisitions of the phantom setup using a 1.5-T clinical magnetic resonance scanner (Avanto, Siemens, Erlangen, Germany) resulting in a time-resolved velocity vector field with a reconstructed spatial resolution of $1.6 \times 1.6 \times 2.1$ mm^3 and temporal resolution of approx. 30 ms. Additionally, we recorded time resolved pressure values with a low-diameter fluid-filled catheter at six locations along the elastic tube with a distance of 50 mm between to adjacent sites.

We calculated the APW from the 4D PC-MRI acquisitions using a vessel section D which covered a length of 150 mm. As a reference value, the global pressure development over one flow cycle was computed by averaging all obtained values from catheterization. As mentioned before, the value for Δd as the spatial resolution of Q and A can be arbitrarily chosen in our software. We investigated the influence of different values of Δd on the accuracy of the computation of the PWV and the APW. Additionally, we evaluated the impact of the two definitions of the pulse arrival time.

The pressure catheter measured the sum of static and dynamic pressure due to its flow-aligned orientation. In contrast, the computation of the APW always delivers static pressure. Therefore, we estimated the dynamic pressure from the aforementioned two-dimensional fields Q and A using the Bernoulli equation. The total APW $p_{total}(t)$ was computed by adding the static APW $p_{stat}(t)$ and the dynamic pressure. The total APW was compared to the catheter measurements after a manual temporal registration. The individual temporal averages were subtracted from all pressure curves since all values are given as relative pressures.

E. In-Vivo Study: Healthy Volunteers

We applied our approach to MRI acquisitions of three healthy volunteers (*Vol1*: 22 years, male; *Vol2*: 23 years, male; *Vol3*: 22 years, female). Ethics committee approval was obtained and all volunteers gave informed consent before investigation. For every volunteer, we acquired the thoracic aorta using the same type of clinical magnetic resonance scanner, MRI sequences and imaging parameters as in the in-vitro experiments. We computed the APW from the 4D PC-MRI acquisitions using a vessel section D which covered the distal aortic arch and the proximal descending aorta. It started at the middle of the aortic arch and had a length of 15 cm. The same algorithmic parameters as in the phantom experiments were investigated and we applied the same steps for the inclusion of the dynamic pressure.

III. RESULTS

A. In-Vitro Study: Experimental Phantom Setup

The pressure values obtained by catheterization showed a temporal delay of approximately 31 ms for the pulse arrival time over a length of 250 mm. This corresponds to a rough estimate of 8.1 m/s for the PWV. The best agreement between the computed PWVs and the reference value was achieved with the *Foot* pulse arrival time and spatial resolutions of $\Delta d < 5$ mm (see Fig. 3).

Fig. 4a) depicts the APWs in the experimental phantom setup. Only the results for the PWV from the *Foot* pulse arrival time are shown. Different spatial resolutions (1 mm $< \Delta d <$ 100 mm) were used for the computation of both the PWV and the APW. A subset of these spatial resolutions are shown in Fig. 4a). For low values of Δd, the range of the pressure curves as well as its detailed shape showed better results. In accordance with the results of Fig. 3, the best agreement with catheterization was achieved with the *Foot* pulse arrival time and with $\Delta d < 5$ mm. This corresponds to the use of 30 analysis planes or more in the vessel section D. These observations were supported by the root mean squared errors between the computed APWs and the catheter measurements (see Fig. 4b)).

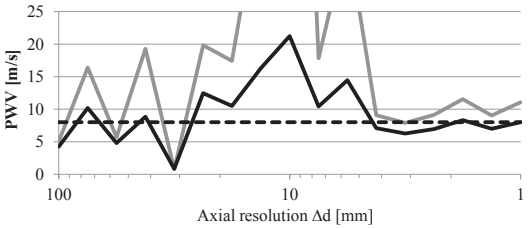

Fig. 3. Catheter-based estimation of the PWV (dashed black) and computed PWVs using the *Foot'* (solid grey) and *Foot* (solid black) pulse arrival times in the phantom setup.

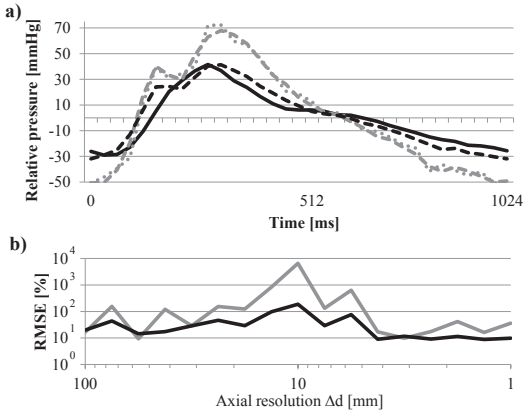

Fig. 4. a) Catheter measurements (solid black) and computed APWs for $\Delta d = 17.5$ mm (grey dots), $\Delta d = 7.5$ mm (dashed grey), $\Delta d = 1$ mm (dashed black) in the phantom setup. b) Root mean squared errors (RMSE) between catheter measurements and computed APWs using the *Foot'* (grey) and *Foot* (black) pulse arrival times. The RMSEs are shown in percent of the APW amplitude.

B. In-Vivo Study: Healthy Volunteers

For the investigated healthy volunteers, the PWV showed physiologically realistic and stable results if values of $\Delta d <$ 5 mm (*Vol1* and *Vol2*) or $\Delta d <$ 10 mm (*Vol3*) were used (see Fig. 5a). Thus, only values of $\Delta d < 5$ mm produced stable results for all investigated volunteers. For the *Foot* pulse arrival time, which showed the best results in the experimental phantom setup, a PWV of 4.6 m/s (*Vol1*), 4.5 m/s (*Vol2*) and 4.9 m/s (*Vol3*) was obtained for the lowest tested Δd of 1 mm.

Fig. 5b) depicts the APWs which were determined based on the previously calculated PWVs in the healthy volunteers. Again, different spatial resolutions (1 mm $< \Delta d <$ 100 mm) were used for the computation of both the PWV and the APW. Only a subset of these spatial resolutions are shown in Fig. 5b). For *Vol1* and *Vol2*, no decision can be made wether the shape of the pressure curves benefits from higher spatial resolutions. The pressure range showed physiologically realistic results for both definitions of the pulse arrival times. The most stable results were achieved

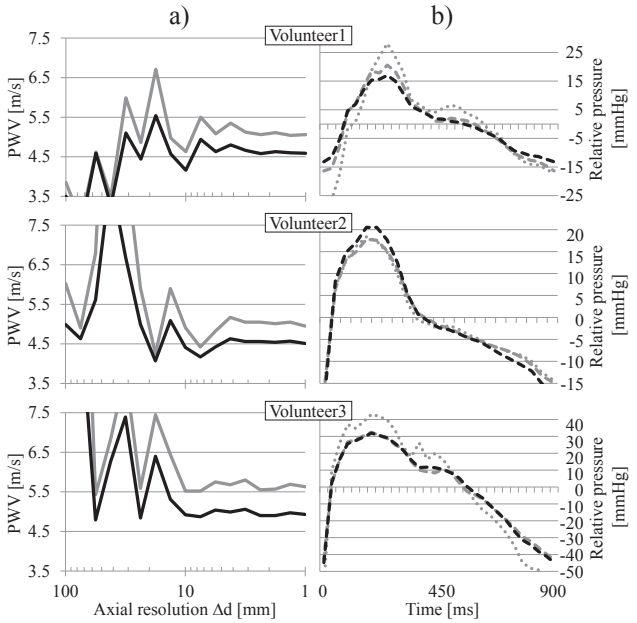

Fig. 5. a) Computed PWVs using the *Foot'* (grey) and *Foot* (black) pulse arrival times in the healthy volunteers. b) Computed APWs for $\Delta d = 17.5$ mm (grey dots), $\Delta d = 7.5$ mm (dashed grey), $\Delta d = 1$ mm (dashed black).

with $\Delta d < 7.5$ mm. For *Vol3*, the shape of the pressure curve showed less spikes and therefore a more physiologically realistic behavior for spatial resolutions of $\Delta d < 13$ mm. The most stable results were achieved with $\Delta d < 10$ mm. On the whole, physiologically realistic and stable results were only achieved in all volunteers if values of $\Delta d < 7.5$ mm were used, which corresponds to the use of 20 analysis planes or more in the vessel section D.

IV. DISCUSSION AND CONCLUSION

The results of our approach agreed well with catheterization in the in-vitro experiments and were physiologically realistic in the in-vivo experiments. We showed that a large amount of cross-sectional analysis planes has to be used in order to overcome the limited 4D PC-MR image quality. These limitations are mainly given by the low temporal resolution, which makes the computation of the PWV and the amplitude of the APW more difficult. Additionally, the low spatial resolution and signal-to-noise ratios affect the information of the cross-sectional vessel area, which defines the shape of the APW. In our experiments, a value of $\Delta d < 7.5$ mm was necessary to produce stable results for the APW in all healthy volunteers, which corresponds to 20 analysis planes in the chosen vessel section. Even more analysis planes would be necessary, if pathologically increased PWVs were present [5]. Therefore, our approach significantly benefits from the automated placement of analysis planes in our software, which minimizes manual effort. This procedure is possible due to the segmentation algorithm [7], which identifies the vessel volume and centerline based on both the morphological information and the tri-directional velocity information of 4D PC-MRI. Compared to a manual placement, this approach not only enables us to use a large amount of cross-sectional analysis planes, it also prevents deviations from the orthogonality to the vessel centerline.

Our work is based on the same principles as the work of Markl et al. [4,5] and Urchuk et al. [2], but differs from these articles in some points. Unlike Markl et al., we compared the computed PWV and APW values to catheter reference measurements. Secondly, the cross-sectional analysis planes had to be placed manually in previous works. Urchuk et al. suggested computing the PWV from a wave equation instead of the delay of pulse arrival times, if MR acquisitions with a low temporal resolution are used. However, in our opinion this method could be error-prone on 4D PC-MRI, since it is based on spatial and temporal derivatives of the blood flow, which suffer from the typically low signal-to-noise ratios.

In conclusion, we presented an approach for the computation of aortic pressure waveforms from phase-contrast magnetic resonance imaging. To our knowledge, this is the first work proposing an approach for the computation of the APW which can be completely performed using 4D PC-MRI. Compared to previous methods for the computation of the APW, our approach has minimal manual effort and can be combined with other 4D PC-MRI-based investigations of blood flow and spatial pressure maps.

REFERENCES

[1] M.C. Langham, C. Li, and F.W. Wehrli, "Non-triggered quantification of central and peripheral pulse-wave velocity," *Journal of Cardiovascular Magnetic Resonance*, vol. 13, no. 1, pp. 1-7, 2011.

[2] S.N. Urchuk, S.E. Fremes, D.B. Plewes, "In vivo validation of MR pulse pressure measurement in an aortic flow model: preliminary results," *Magnetic resonance in medicine*, vol. 38, no. 2, pp. 215-223, 2005.

[3] J. Tyszka, D. Laidlaw, J. Asa, and J. Silverman, "Three-Dimensional, Time-Resolved (4D) Relative Pressure Mapping Using Magnetic Resonance Imaging," *Journal of Magnetic Resonance Imaging*, vol. 12, no. 2, pp. 321-329, 2000.

[4] M. Markl, W. Wallis, S. Brendecke, J. Simon, A. Frydrychowicz, and A. Harloff, "Estimation of global aortic pulse wave velocity by flow-sensitive 4D MRI," *Magnetic Resonance in Medicine*, vol. 63, no. 6, pp. 1575-1582, 2010.

[5] M. Markl, W. Wallis, C. Strecker, B.P. Gladstone, W. Vach, and A. Harloff, "Analysis of pulse wave velocity in the thoracic aorta by flow-sensitive four-dimensional MRI: Reproducibility and correlation with characteristics in patients with aortic atherosclerosis," *Journal of magnetic resonance imaging: JMRI*, vol. 35, no. 5, p. 1162, 2012.

[6] S. Seifert, R. Kussaether, W. Henrich, N. Voelzow, and R. Dillmann, "Integrating Simulation Framework MEDIFRAME," *Proceedings of the 25 IEEE Engineering in Medicine and Biology Conference*, pp. 1327-1330, 2003.

[7] M. Schmidt, R. Unterhinninghofen, S. Ley, and R. Dillmann, "Flow-based segmentation of the large thoracic arteries in tridirectional phase-contrast MRI," *Proc. SPIE Medical Imaging*, vol. 7259, pp. 725914, 2009.

[8] M. Stevanov, J. Baruthio, D. Gounot, and D. Grucker, "In vitro validation of MR measurements of arterial pulse-wave velocity in the presence of reflected waves," *Journal of Magnetic Resonance Imaging*, vol. 14, no. 2, pp. 120-127, 2001.

[9] M. Delles, F. Rengier, S. Ley, H. von Tengg-Kobligk, H.-U. Kauczor, R. Unterhinninghofen, and R. Dillmann, "Influence of imaging quality on magnetic resonance-based pressure gradient measurements," *Proc. SPIE Medical Imaging*, vol. 7626, p. 762624, 2010.

[10] F. Rengier, M. Delles, R. Unterhinninghofen, S. Ley, M. Müller-Eschner, S. Partovi, P. Geisbüsch, R. Dillmann, H.U. Kauczor, and H. von Tengg-Kobligk, "In vivo and in vitro validation of aortic flow quantification by time-resolved three-dimensional velocity-encoded MRI," *The International Journal of Cardiovascular Imaging (formerly Cardiac Imaging)*, pp. 1-10, 2012.